UNIVERSITAT POLITÈCNICA DE CATALUNYA

Laboratory of Photonics
Electromagnetics and Photonics Engineering group
Dept. of Signal Theory and Communications

OPTICAL SOLITONS IN QUADRATIC NONLINEAR MEDIA AND APPLICATIONS TO ALL-OPTICAL SWITCHING AND ROUTING DEVICES

Autor: María Concepción Santos Blanco
Director: Lluís Torner

Barcelona, january 1998

Chapter 7

Topological Switching

A rigorous treatment of steering issues in 2+1 configurations would certainly require an analysis of the kind of the one carried out for the 1+1 setups with the added complexity of having to deal with two transverse variables. However no substantially different effects from those observed in the 1+1 case are likely to be obtained which would make worth the effort here. Instead, we shall concentrate on an interesting case which has not an equivalent in 1+1 setups, namely propagation of *optical vortices.*

Optical vortices characterized by an spiral dislocation of the phase-front that has an helical phase-ramp around a phase singularity, owe their interest mainly to the fact that they are rather easily generated experimentally and provide simple ways to interprete the results. The dynamics of optical vortices has been investigated in both linear and cubic nonlinear media by several authors [156]-[167].

It has already been stressed the key role played by the initial relative phase between harmonics in the dynamics of soliton formation. That is so to the point that if the input contains different transverse zones affected by different relative phases, they may evolve independently so that solitons form in zones in which the initial relative phase favours the dynamics, stealing away some energy from these zones in which the initial relative phase is against soliton formation so that the net result is that the input beam becomes splitted up into several solitons formed in more favoured zones.

The goal in the present chapter is to numerically investigate in 2+1 geometries the splitting up effect due to transverse relative phase differences into the input beam in the form of

optical vortices, with eyes to a practical demonstration which takes advantage of the simple experimental setups provided by these geometries.

Specifically, as a first case it is considered the beam evolution in bulk crystals when both the fundamental and second harmonic input beams are Gaussian, but the second harmonic beam contains a vortex nested in its center. Depending on the input light conditions, the beams will be shown to either form a single soliton or self-split into several solitons. Both the origin of the splitting and how the number of output solitons depends on the input light intensities and on the topological charge of the phase dislocation are discussed and a brief study of the effects introduced by a wavevector mismatch and the presence of Poynting vector walk-off is included as well.

The second case is second harmonic generation, i.e. the input consists only of a fundamental beam with a phase dislocation. In this case the process of second harmonic generation becomes unstable against azimuthal modulations. Numerical simulations were carried out for initial conditions including a small random noisy field for the study of this effect.

7.1 Optical vortices: field distribution and methods of generation

Usually beams with a phase dislocation are referred to as an optical vortices. Optical vortices and their associated dynamics in both linear and cubic nonlinear media have been investigated by several authors in the last few years, [157], [166], [167], and they have been shown to display interesting properties with potential applications. In particular, Tikhonenko and co-workers observed experimentally the break-up of a modulationally unstable vortex into bright solitons in saturable self-focusing cubic nonlinear media, [166], [167], a phenomenon somehow similar to the splitting studied here.

Through the use of appropriate phase masks or by transformation of Hermite-Gaussian modes with astigmatic optical components [168], [169], [170], Laguerre-Gaussian beams which include a phase singularity provide a rather easy way of experimental optical vortex generation.

Formally, the field of a Laguerre-Gaussian beam propagating along the $z-$axis is given by

$$a(r_\perp, z) = A\, r_\perp^{|m|} \exp(im\varphi) L_p^m(\frac{2\,|r_\perp|^2}{w^2}) \exp(-\frac{|r_\perp|^2}{w^2}), \tag{7.1}$$

where $r_\perp$ is the transverse radius-vector, L_m^p is the Laguerre polynomial, w is the beam width, A is the beam amplitude, $\varphi = \tan^{-1}(\mathrm{Im}(r_\perp)/\,\mathrm{Re}(r_\perp))$ is the azimuthal angle and m is the topological charge of the phase dislocation. In this study the values $m = 1$ or 2, and $p = 0$ or $p = 1$ so that the fields have cylindrical symmetry and have one or two nodes are considered. The corresponding Laguerre polynomials are $L_0^1 = L_0^2 = 1$; $L_1^1 = 2 - \frac{2|r_\perp|^2}{w^2}$; $L_1^2 = 3 - \frac{2|r_\perp|^2}{w^2}$.

Figure 7-1 features an sketch of two simple ways for experimental generation of such beams. When the pattern showed in Figure 7-1 (a) is illuminated with coherent light, the first diffraction order produced has helical wave front with phase singularities that show up as defects in the fringes pattern of the interference between this beam and a non collinear plane wave.

Another way to generate Laguerre-Gaussian beams with phase singularities uses the Hermite-Gaussian output of a conventional laser and its transformation into the corresponding Laguerre-Gaussian beam. Figure 7-1 (b) shows the principle of this transformation. A Hermite-Gaussian mode HG_{01} can be generated using a conventional laser if a crosswire is inserted into the laser cavity. To produce a $\pi/2$ phase shift a cylindrical lenses mode convertor may be used [169]-[170].

With illustrative purposes and because the interest is lied mainly in identification of effects and possibilities the numerical simulations consider the 2+1 governing equations for the formally simpler Type I (2.97) phase matching geometries.

Since the study considers input conditions without azimuthal symmetry, to the usual three conserved quantities which are useful to monitor and describe the beams evolution, a fourth quantity is added, namely the longitudinal component of the total angular momentum of the light beams given by $L = \int \left[\vec{r}_\perp \times \vec{\mathcal{J}}_2\right]_z dr_\perp$, with $\vec{\mathcal{J}}_2$ being the transverse beam momentum associated with the second harmonic wave. In absence of Poynting vector walk-off, L is also a conserved quantity of the beam evolution. When walk-off is present, one readily finds that

$$\frac{dL}{d\xi} = \left[\vec{\delta} \times \vec{\mathcal{J}}_2\right]_z . \tag{7.2}$$

For the right-hand-side of this equations to vanish in the presence of walk-off, the transverse

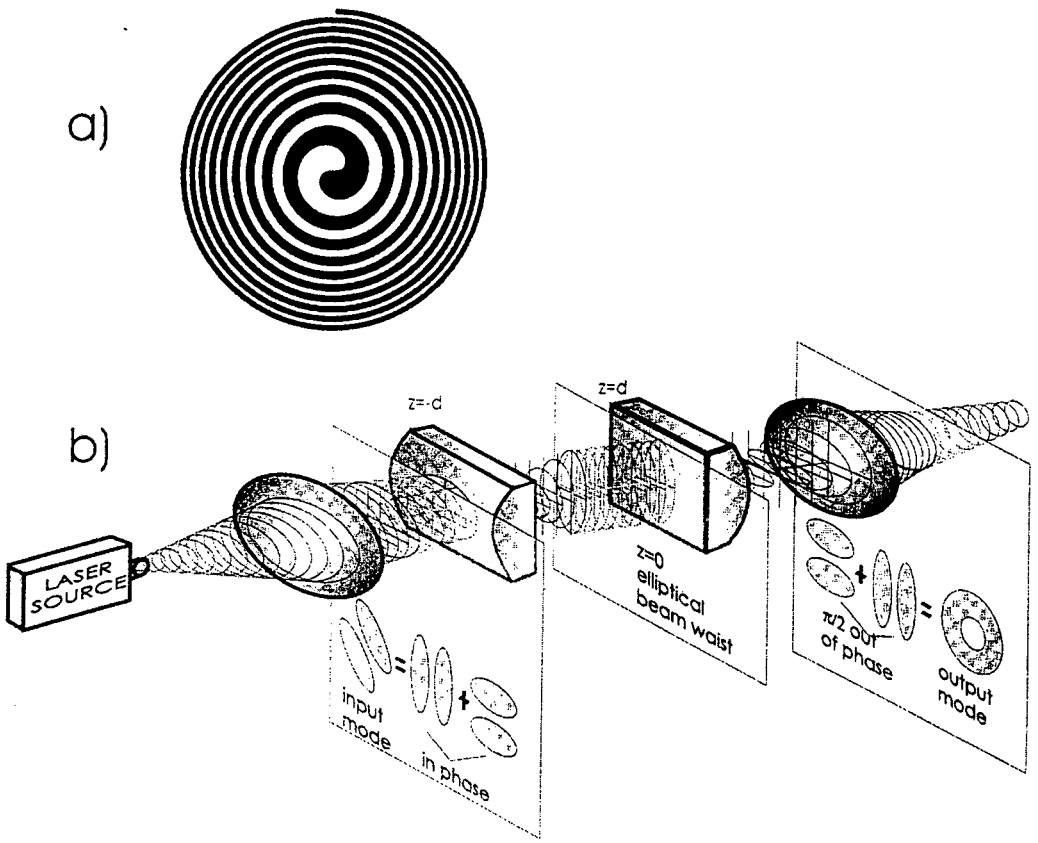

Figure 7-1: a) Computer-generated zone plates with $m = 1$. b) The cylindrical lens mode convertor. If the input $HG_{1,0}$ mode is oriented at 45^o with respect to the cylinder axis of lens the mode is converted into the LG_0^1 mode.

momentum of the second-harmonic beam $\vec{\mathcal{J}}_2$ has to be parallel to $\vec{\delta}$, and such is the case when input light beams with azimuthal symmetry or with a phase-front tilt are considered [122]-[123], [119]. Otherwise, as it is the situation studied here, the total angular momentum is not conserved in the presence of Poynting vector walk-off.

To analyze the evolution of charge at the phase singularity (i.e., the value of m) in the beams of both frequencies, the interference fringes arising by mixing the normalized calculated fields at a given distance ξ with a reference plane wave slightly tilted relative to the propagation axis were considered. The tilt is towards the x axis. The resulting intensity from such an interference is now

$$I_{int} = \left| \frac{a_{1,2}(r_{\perp x}, r_{\perp y})}{|a_{1,2}(r_{\perp x}, r_{\perp y})|} + \exp(ik_x r_{\perp x}) \right|^2 , \tag{7.3}$$

where k_x is the spatial frequency of the tilted plane wave used as reference. The value of k_x is chosen for each field distribution to have good spatial resolution. Thus, a phase singularity appears as a dislocation, and a topological charge m is visually evaluated.

To monitor the formation and evolution of spatial solitons the Hamiltonian $\mathcal{H}$, the components of transverse momentum $\mathcal{J}_x$ and $\mathcal{J}_y$, and the angular momentum L_z relevant to a particular solitary wave were computed by using the fields in the vicinity of the given solitary wave.

7.2 Numerical experiments

To investigate the effect of the angular momentum associated with azimuthal symmetry breaking on the beam evolution, several numerical experiments solving eqs. (2.97) with a split-step Fourier algorithm were performed for a variety of input beam shapes and material conditions. The outcome of the simulations obtained by taking Gaussian input beams with a phase dislocation nested in the second harmonic is next presented.

The inputs considered have generically the form

$$\begin{aligned} a_1(\xi = 0, r_\perp) &= A \exp(-r_\perp^2/w_1^2), \\ a_2(\xi = 0, r_\perp) &= B r_\perp^{|m|} \exp(im\varphi) \exp(-r_\perp^2/w_2^2), \end{aligned} \tag{7.4}$$

where φ is the azimuthal angle in cylindrical coordinates, the integer m is the topological charge of the phase dislocation, and $\mathrm{sgn}(m)$ its chirality. In all simulations presented it is set $w_1 = w_2 = 2$. Notice that the input beams (7.4) carry the angular momentum $L = mI_2$, and that for a given amplitude B the power carried by the second-harmonic beam, I_2, is different for each value of $|m|$.

With the purpose of elucidating the impact of the topological charge of the phase dislocation on the beam evolution, the case of phase-matching ($\beta = 0$) in the absence of Poynting vector walk-off ($\delta = 0$) is examined in the first place. Figure 7-2 shows the summary of the output of a series of numerical experiments that display the main features of the beam evolution. The plots show the fundamental beams at $\xi = 12$, for different values of the charge of the vortex in the second-harmonic input beam. The features of the second-harmonic fields are similar and thus not shown. The amplitudes of the beams A and B have been taken to be well above threshold for single soliton formation [87]-[89] and B has been chosen to yield similar values of I_2 regardless of the value of m. The results shown in Figure 7-2 are representative of the effects that occur over a range of input light conditions, but it is worth recalling that the precise pattern of output beams does depend on the value of the various parameters involved, and in particular on the input light intensity, as it shall be shown and discussed shortly. In the absence of the phase dislocation, the beams mutually trap and form one soliton as shown in Fig. 7-2(a). However, Figs. 7-2(b)-(d) show that when $m \neq 0$, the helical phase-front of the second-harmonic input

produces the splitting of the beams into several solitons. It has been verified that the fraction of the total Hamiltonian carried by each outgoing soliton amounts to a negative value, in agreement with the energy flow-Hamiltonian relation of the family of stationary soliton solutions [87]-[89]. The solitons emerge in different directions carrying different individual transverse momenta. Recall that the total transverse momentum $\vec{J}$ is conserved and that some fraction of it is in the form of radiation.

The total angular momentum L is also conserved. Therefore, either the pattern of output beams rotates during propagation or the relative phases of the several output solitons have to be different so that there is an azimuthally-asymmetric phase distribution. Under most conditions studied, and in particular in all cases shown here, the latter was observed to be indeed the case. This fact might be partially responsible of the mutual repulsion that makes adjacent solitons to separate from each other.

The pattern of the interference fringes indicate no phase singularity in the fundamental beam and dislocations with a charge $m = 1, 2$ or 3 in the input second harmonic beam, depending on the charge of the initial vortex (Fig.7-3). After some propagation distance a break-up of the defects with $m \neq 1$ into single-charge defects with the same sign is observed in the second harmonic beam while the fringes pattern for the fundamental beam remains practically unaltered. The break-up of the topological charge in the case $m > 1$ may be explained by a known effect in cubic nonlinear media: the addition of coherent fields induces splitting of a dislocation of charge m into $|m|$ single charge dislocations [161]-[164].

One salient point of Fig. 7-3 is that, for the specific conditions chosen, the number of solitons formed is equal to twice the charge of the vortex. This conclusion also holds for higher values of m than those shown here, provided the input light intensity is high enough so that the $2m$ solitons can be formed dynamically by the process of beam splitting. This requires that the input light intensity is well above the threshold for the existence of $2m$ solitons, because the dynamics of the beam evolution produces dispersive waves that take energy away.

The self-splitting of the beams shown is due to the different dynamics experienced by the portions of the beams located at different azimuthal regions, as follows. Because of the helical phase-front of the second-harmonic input beam, the portions of the two interacting, fundamental and second-harmonic beams located in the different azimuthal positions experience a different

phase relation and therefore undergo different dynamics. As a consequence, the beams split and, in those azimuthal regions where the particular initial dynamics favours the mutual trapping of the beams a soliton is formed. Otherwise, the corresponding portions of the beams tend to spread, and be either radiated or transferred to the regions where a soliton is formed. Of course, the actual beam evolution in either of the above regions depends on the light intensity.

The partition of the beam dynamics into separate azimuthal pieces is readily exposed by examining the initial rate of interharmonics energy exchange between two cylindrically symmetrical, but out-of-phase input beams see (2.113, 2.114) and the analysis in section 6.2. By and large, for the amplitudes relations and wavevector mismatches considered in this study, which approach those for solitary wave propagation, in-phase input beams (i.e. having $\phi_0 = 0$) form solitons much more easier than inputs with a phase difference of π [87]-[89]. Thus in the case studied here, in general solitons tend to form nearby the regions where the input beams are in-phase whereas the portions of the beams that experience a π initial phase difference tend to spread. Also, the beam evolution is not symmetric around $\phi_0 = 0$. In particular, according to (2.113, 2.114), input beams with a positive phase difference, say $|\phi_0|$, start transferring power from the fundamental to the second harmonic, whereas input beams with the same phase difference but with a negative value, i.e. $-|\phi_0|$, start transferring power from the second harmonic to the fundamental. Therefore, a different dynamics is generated at either side of $\phi_0 = 0$.

Naturally, the dynamics of the beam evolution depends a great deal on both the total and the relative input light intensities launched at each frequency. Figures 7-4 to 7-7 show the fundamental beams at $\xi = 10$, for different representative input light intensities with fixed topological charges of the phase-dislocation. In Figures 7-4 and 7-5 it is set $m = 1$ and in Figures 7-6 and 7-7, $m = 2$. In Figures 7-4 and 7-6 the intensity of the fundamental beam is kept fixed whereas the intensity of the input second-harmonic beam varies, and viceversa for 7-5 and 7-7. The plots show that, as expected on physical grounds, the precise pattern of output solitons is sensitive to the input intensities, mainly at the regime of lower input light intensities. For instance, in Figure 7-4(a) the input power is not high enough to allow the dynamical formation of two solitons by the splitting of the input beams, therefore the output pattern is clearly different than the output obtained in the conditions in Figures 7-4(b)-(d).

For the objectives pursued in this study, the main conclusion to be raised from the Figures is

that they clearly confirm the robustness of the self-splitting process, as it happens over a range of conditions producing a reasonably uniform output pattern. Thus, the effect holds promise for experimental exploration.

The dynamics and result of the beam splitting also depend on the material and linear wave propagation conditions, namely the wavevector mismatch and Poynting vector walk-off between the interacting beams, as so does the formation of solitons in the simpler case of cylindrically symmetric beams [87]-[89]. In particular, the soliton properties themselves, e.g. the fraction of power carried by each of the two waves forming the soliton, are different at positive and negative wavevector mismatch. All this impacts strongly the details of the beam splitting process but under appropriate input light conditions the number of output solitons is also given by the results obtained at phase-matching and described above. As a representative example, Fig. 7-8 shows the output solitons obtained at $\beta = \pm 3$ for the same conditions as in Fig. 7-2(b).

Beam splitting into several solitons similar to the phenomenon predicted here also occurs when only a fundamental beam with a variety of ring-like beam shapes, including phase dislocations nested in a Gaussian, higher-order Laguerre-Gaussian beams or general laser doughnut modes, are considered as the input light conditions. Notice that this is an important point from a practical point of view, because the experimental set-up required is simpler than the situation reported here. In such case the beams self-split because of the azimuthal modulational instability of the flat top of the ring-shaped beams, [114]-[115] a process similar to the break-up of analogous beams in saturable cubic nonlinear media [166]-[167], [171]-[172]. Therefore, this process has both a different interpretation and a different dynamics than the splitting studied here and thus requires a separate detailed investigation.

Next it is considered that only a single-charged vortex beam at the fundamental frequency is launched into the crystal. In this case, the ring-shaped beams at both ϖ and 2ϖ are modulationally unstable, thus to 'seed' the instability a small, noisy field is added to the input conditions. It is assumed that the noise induces both amplitude and phase fluctuations, so that the input field is

$$\begin{aligned} a_1(\xi = 0, r_\perp) &= A r_\perp \exp(i\varphi) \exp(-\tfrac{r_\perp^2}{w^2})(1 + R) \\ a_2(r_{\perp x}, r_{\perp y}, \xi = 0) &= 0 \end{aligned} \tag{7.5}$$

where R is the random complex number sequence. The random sequence is assumed to have

zero average, and a uniform distribution in the range $[-1, 1]$. In the numerical experiments a scale factor was used which gives a variance of 10^{-2}. The random sequence was generated by a standard pseudo-random number generator [138]. The noise simulates fluctuations in the input beam that always exist by experimental realization of the SHG and 'seeds' the azimuthal modulational instability.

Several numerical simulations were carried out which considered different realizations of the noise term. In all cases beam break-up into three solitons was observed at $\xi = 10$ (Fig. 7-9). Notice that in this case a generation of the topological defects $2m$ in the second harmonic field is observed. (Fig. 7-10).

As summary, it has been shown numerically that focused light beams with a spiral phase dislocation propagating in bulk quadratic nonlinear crystals self-split into several spatial solitons. The self-splitting process occurs in a wide variety of conditions, including second-harmonic generation settings that involve ring-shaped input beams. Through consideration of simple situations, it was shown that the number and pattern of output solitons can be controlled by the material and wave parameters involved, and in particular by the input light intensity and by the topological charge of the dislocation. The self-splitting process predicted requires experimental features similar to the formation of single solitons, [103]-[119] hence it holds promise for experimental demonstration.

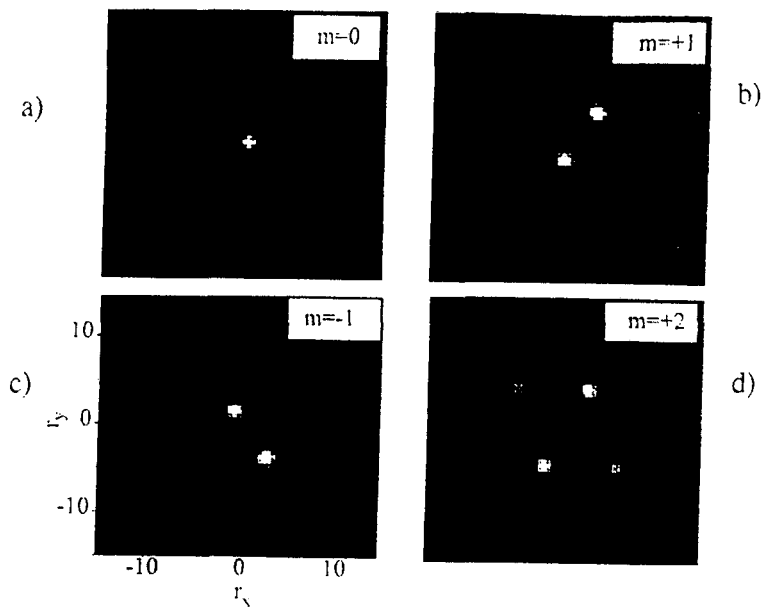

Figure 7-2: Fundamental beams after propagating up to $\xi = 12$ in a phase-matched configuration ($\beta = 0$), for different values of the charge of the phase dislocation of the second-harmonic input beam. The features shown are similar for the existing second-harmonic beam and have not been plotted. (a): $m = 0$, $A = 3$, $B = 5$; (b): $m = 1$, $A = 3$, $B = 4$; (c): $m = -1$, $A = 3$, $B = 4$; (d): $m = 2$, $A = 3$, $B = 2$. In all cases $\delta = 0$.

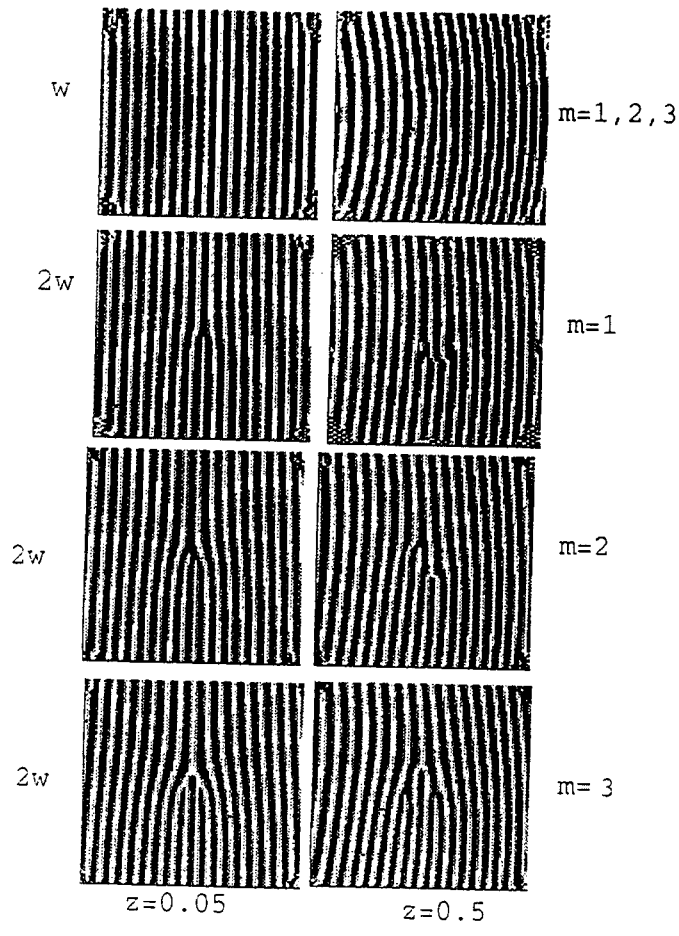

Figure 7-3: Interference fringes obtained by illuminating the fundamental and second harmonic beams with a plane wave tilted with relation to the propagation direction

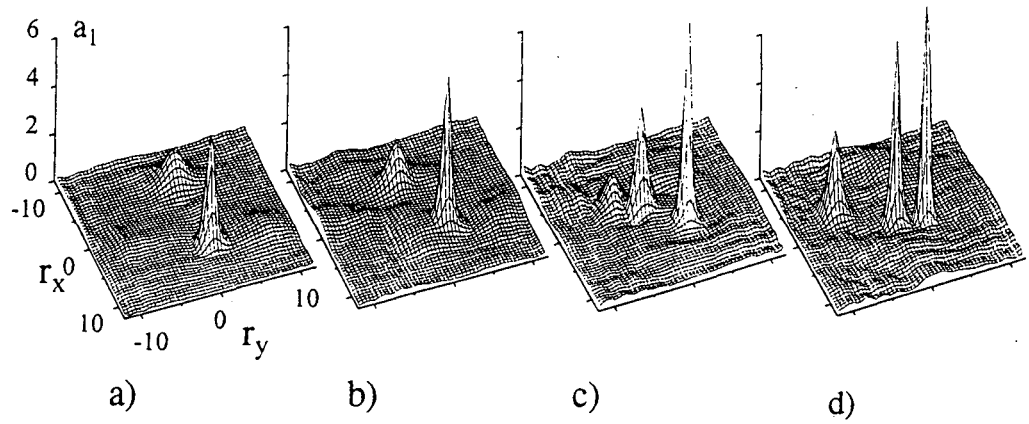

Figure 7-4: Fundamental beam after propagating up to $\xi = 10$ in a phase-matched configuration, for different values of the input light intensities with a fixed value of the phase dislocation of the second-harmonic input beam. In all cases $m = 1$ and $A = 3$. In (a): $B = 2$, in (b): $B = 3$, in (c): $B = 4$, and in (d): $B = 5$.

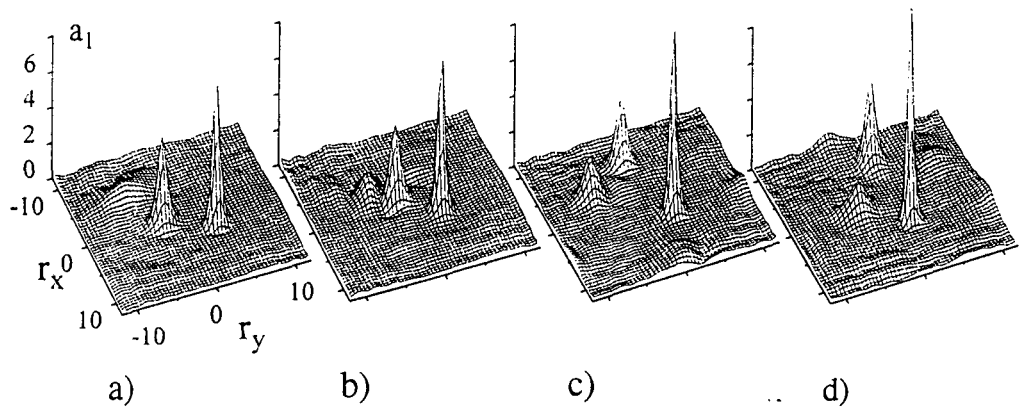

Figure 7-5: Same as in previous figure, but for different input conditions. Here, in all cases $m = 1$ and $B = 4$. In (a): $A = 2$, in (b): $A = 3$, in (c): $A = 4$, and in (d): $A = 5$.

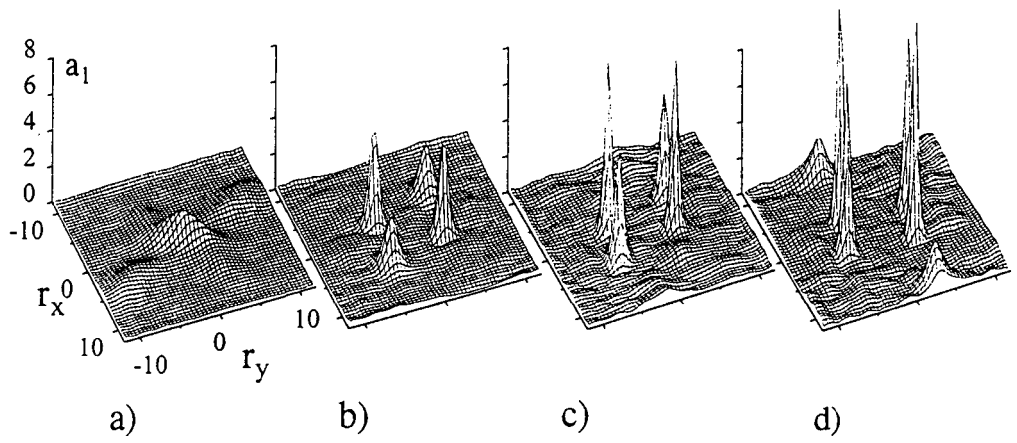

Figure 7-6: Same as Figure 7-4, but for different input conditions. Here, in all cases $m = 2$ and $A = 3$. In (a): $B = 1$, in (b): $B = 2$, in (c): $B = 3$, and in (d): $B = 4$.

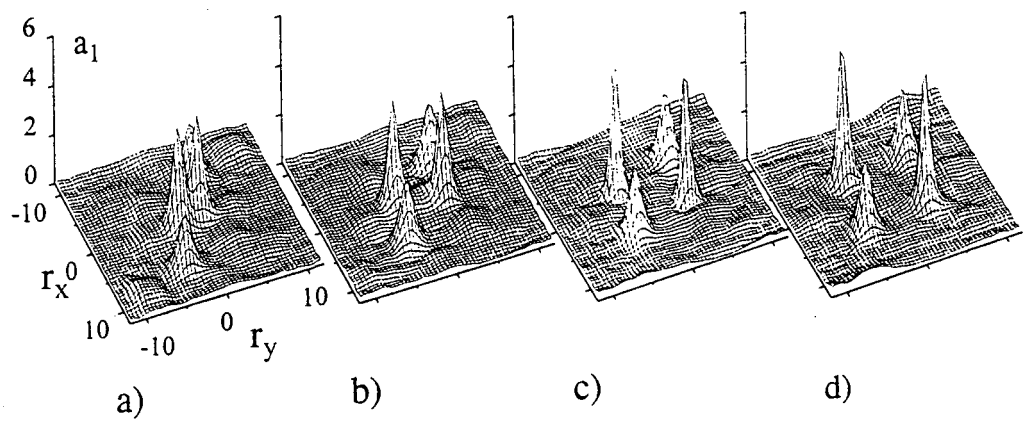

Figure 7-7: Same as Figure 7-4, but for different input conditions. Here, in all cases $m = 2$ and $B = 2$. In (a): $A = 1$, in (b): $A = 2$, in (c): $A = 3$, and in (d): $A = 4$.

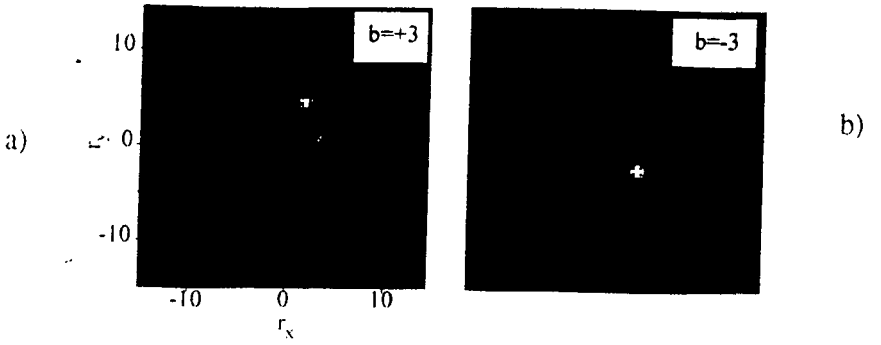

Figure 7-8: Same as in Fig. 7-2(b), but at positive and negative wavevector mismatch. (a): $\beta = 3$; (b): $\beta = -3$. In both cases $m = 1$, $A = 3$, $B = 4$, and $\delta = 0$.

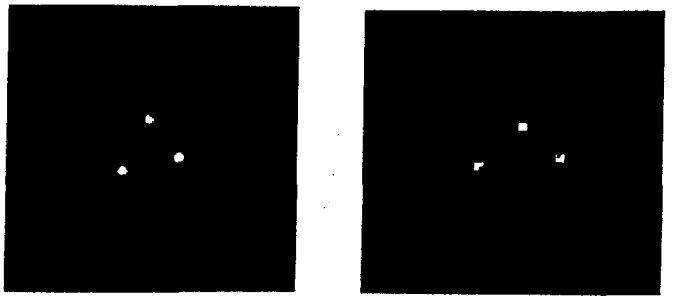

Figure 7-9: Fundamental beam after propagation up to $\xi = 10$ by SHG with an initial amplitude and $A = 6$ for two realizations of the noise term .

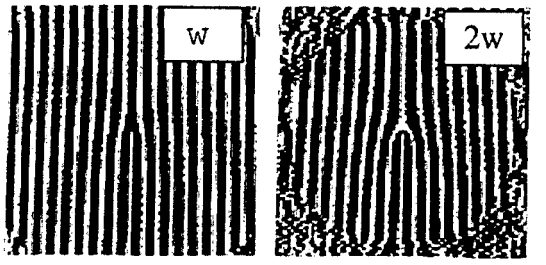

Figure 7-10: Interference fringes for the fundamental beam and double frequency beam in previous Figure.